

Exploring the effect of lithium-ion content on the electrochemical performance of commercial aluminum anodes in alkaline batteries

Mohamed Abdelsamie^{1*}, Abdelrahman Elsayed¹, and Mahmoud Elrouby^{1,2*}

¹ Chemistry Department, Faculty of Science, Sohag University, Sohag, 82524, Egypt

² King Salman International University, Faculty of Science, Ras Sudr, Sinai, 46612 Egypt

Received: 16 Mar. 2022, Revised: 11 Apr. 2022, Accepted: 18 Apr. 2022.

Published online: 1 May 2022

Abstract: This research aims to find the best solution/material interface for improving the performance of alkaline Al-air batteries. It is found that the small addition of LiOH to a NaOH solution makes a great change in the electrochemical performance dramatically. In both 1M NaOH and 1M (90 percent NaOH + 10 percent LiOH) solutions, the corrosion behavior of aluminum and hence the Al-air battery performance were examined. The results reveal that the commercial aluminum electrode gains superior electrochemical characteristics under optimized conditions. It has a better electrochemical performance in the 1M (90 percent NaOH + 10 percent LiOH) solution. Moreover, higher anodic passivation and a lower corrosion rate than the pure 1M NaOH solution were observed. It is found that the corrosion products morphology of aluminum progresses from intergranular to uniform corrosion. The results of the scanning electron microscope (SEM) and electrochemical impedance spectroscopy (EIS) are in good agreement with electrochemical performance.

Keywords: Commercial aluminum; corrosion; electrochemical performance; lithium-ions; alkaline batteries.

1 Introduction

With the increasing consumption of fossil energy and the aggravation of environmental pollution, the metal-air battery has aroused great interest in the field of energy. This is because of its unique advantages of high theoretical energy density, rich energy storage [1], and low cost compared with numerous primary and rechargeable batteries, such as Li-ion, Ni-Cd, and lead-acid batteries. It is well known that aluminum is an attractive candidate anode material for metal-air batteries, primarily due to its inherent properties, including the high theoretical volumetric energy capacity of 8046 mAh cm⁻³ [2-4]. Furthermore, its high theoretical gravimetric energy capacity of 2980 mAh g⁻¹ is higher than those of other active metals, such as Mg (2.20 Ah g⁻¹) and Zn (0.82 Ah g⁻¹). Also, its negative standard electrode potential (2.31, 2.30, 1.68 V vs. saturated hydrogen electrode (SHE) in alkaline, neutral, acid electrolyte). Aluminum is the third most abundant element in the earth's crust (8.8 wt. %), as well as a production low cost [5-6]. However, Al can be automatically oxidized by oxygen in the air and in an aqueous solution to form a protective alumina film on its surface. Accordingly, the corrosion potential of the Al anode shifts positively. Then the discharge performance of the Al electrode can be greatly limited, causing a significant

loss of the available energy. In order to overcome this challenging issue, alkaline NaOH solution as an electrolyte is often used in the Al-air battery since the oxide film can be dissolved easily in an alkaline solution.

Nevertheless, two main issues are usually associated with the usage of alkaline solutions. One is the serious self-corrosion of Al anode during the discharging process, leading to the columbic loss on discharge and fuel loss during standby. The other one is forming a passive hydroxide layer on the Al anode surface, resulting in the decrease of electrochemical activity [7]. This work aims to improve the electrochemical activity and retarding the corrosion rate of the commercial aluminum electrode by adding a minor percentage of Li ions to the NaOH solution.

2 Experimental

2.1. Materials and electrolytes preparation

The fusion method prepared the aluminum electrode, where commercial aluminum blocks were placed in a high-purity graphite crucible at 740°C in a muffle furnace. Molten metal was cast into a stainless-steel mold (200 mm x 180 mm x 25 mm). In comparison, pure Al ingot was also cast via the same procedures. Afterward, the as-cast bars were given a homogenizing heat treatment at 500 °C for 8 h

* Corresponding author E-mails: mhmd2018100@gmail.com , dr_mahmoudelrouby@hotmail.com

and cooled inside the furnace to room temperature. Al plates were produced by hot rolling the ingot to 10 mm at 420 °C and then cold rolling to 3 mm in multi-pass, followed by annealing at 400 °C for 2 h and subsequent air cooling. Annealing is needed to reach the physico-chemical equilibrium and improve mechanical properties [8-9]. Finally, Al specimens were cut into cuboids of equal sizes and wetly polished with 400 - 1500 grit size silicon carbide papers before tests. The existing phases were identified using an X-ray diffractometer (XRD) and scanning electron microscope (SEM). The elements' percentages were determined using energy dispersive spectroscopy (EDX). The electrolyte solutions were 1M NaOH and 1M (90 percent NaOH + 10 percent LiOH) solutions. The solutions were prepared using double distilled water (specific resistance $\geq 18.25 \text{ M}\Omega \text{ cm}$).

2.2. Characterization

The synthesized electrodes' structural phases were identified using a Bruker AXS-D8 advanced X-ray diffractometer (XRD). The morphology of the working electrodes and the percentages of elements in the synthesized electrodes was examined by utilizing a JEOL-5300 scanning electron microscope (SEM) provided with EDX unit.

2.3. Electrochemical measurements

The electrochemical measurements were accomplished in a pyrex glass cell of three electrodes using VersaSTAT4 potentiostat/galvanostat. The electrochemical experiments were achieved via disk electrodes (Al) embedded in an Araldite holder as a working electrode. Before immersion in the polarization cell, the electrodes were polished with sequacious grades of emery paper, degreased in pure ethanol, and washed in running bi-distilled water. A counter electrode of a platinum sheet has been used. A saturated silver/silver chloride (Ag/AgCl) was utilized as a reference electrode to which all potentials were compared. The surface of working electrodes was cleaned from residual grease and other oxides by applying a constant potential at -1.5 V for 5 min in both 1M NaOH and 1M (90 percent NaOH+10 percent LiOH) solutions. Then the electrode was disconnected and shaken to remove the adsorbed hydrogen bubbles on the electrode surface. After that, the cathodic and anodic polarization measurements were recorded [10-12].

2.3.1. Tafel and Potentiodynamic polarization

The cathodic and anodic Tafel plots were performed at a potential scan rate of 1 mV/s, within a potential range of +0.25 and -0.25 V regarded to the E_{corr} (corrosion potential). A potential range of 1.6 and -2.5 V regarded to the E_{corr} was applied for the polarization test.

2.3.2. EIS measurements

The EIS experiments were accomplished by applying direct DC potentials of -100 and +100 mV, Ac potential amplitude of 10 mV, and frequencies ranging from 10 kHz to 1 Hz.

2.4. Evaluation of the corrosion parameters

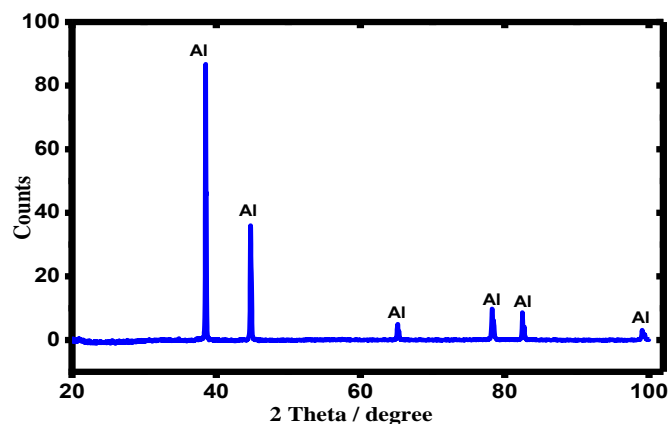
The working electrodes were allowed to equilibrate in 1M NaOH and 1M (90 percent NaOH+10 percent LiOH) solutions for 30 min at the corrosion potential (E_{corr}). The current densities of corrosion (I_{corr}) for the investigated electrodes were accurately detected by determining the intersection point of extrapolated cathodic and anodic Tafel lines. All experiments were achieved by using a recently prepared solution and polished electrodes. The experiments were repeated two or three times, and reproducibility was satisfactory.

3 Results and discussion

3.1. Characterization of the prepared electrodes

3.1.1. XRD technique

Fig. 1 exhibits the patterns of XRD for the commercial Al, which indicates six characteristic peaks for the aluminum as a cubic crystalline structure. The six distinct peaks are convenient with that of JCPDS Cards: 85-1324 [9]. The values of crystal parameters, Millar indices, 2



thetas, and displacing are listed in Table 1.

Fig. 1. Patterns of XRD for Al electrode

Table 1: The XRD data of the Aluminum electrode.

Electrode	Crystal system	d (Å ^o)	2θ (degree)	I fix	h	k	l
Al	Cubic	2.33600	38.507	1000	1	1	1
		2.02300	44.763	470	2	0	0
		1.43050	65.161	264	2	0	2
		1.21990	78.314	278	3	1	1
		1.16800	82.524	78	2	2	2
		1.01150	99.201	37	4	0	0

It is clear from table 1 that phase (111) is the main phase and then the (200) phase.

3.1.2. SEM imaging and EDX analysis

Fig. 2 shows the scanning electron microscope image of the Al surface electrode. The surface seems to be scratched with vertical lines due to polishing. It could be shown that the entire Al surface was rough and consisted of irregular spots. Furthermore, from the images at different magnifications, it can be noted that there are many phases on the surface of the electrode. These phases may be attributed to the formation of oxides due to the activity of the Al electrode surface and other impurities [13-15]. (EDX) analysis for the Al sample is shown in Fig. 2 and Table 2. From these data, it can be noted that the presence of Al is the major content of about 86%, and oxygen is the second major element of percent, about 12%. 2% for the other elements as Cl, Na, and Ca are shown in Table 2 and Fig. 2. This confirms the interpretation of the SEM images and XRD data.

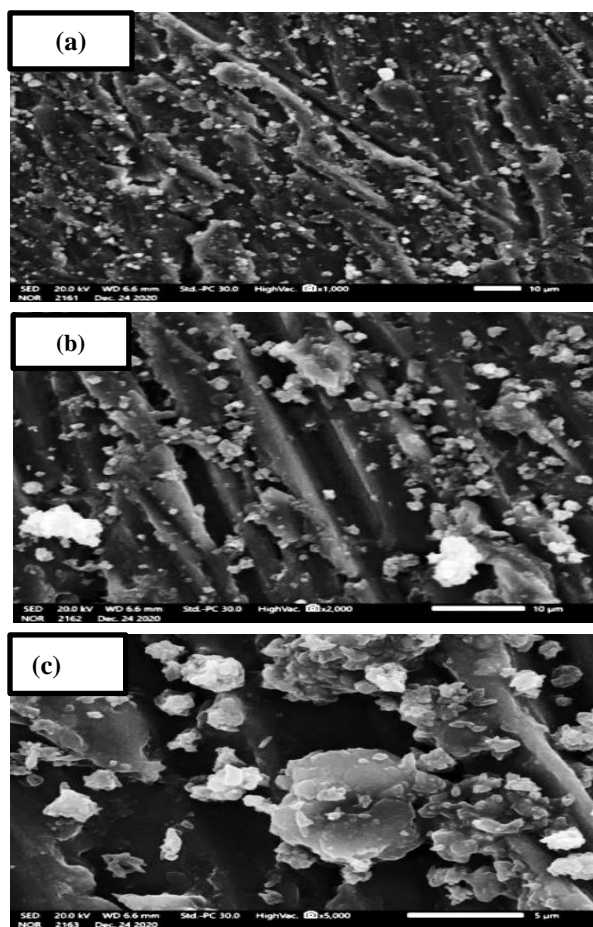


Fig. 2. SEM images of the pure surface of Al (a) at a magnification of $\times 1000$, (b) at a magnification of $\times 2000$, and (c) at a magnification of $\times 5000$.

Table 2: EDX analysis for the Al surface.

Electrode	Element	Mass%	Atom%
Al	O	7.27 ± 0.18	11.74 ± 0.29
	Na	0.73 ± 0.05	0.82 ± 0.05
	Al	89.80 ± 0.39	85.98 ± 0.37
	Cl	0.50 ± 0.05	0.37 ± 0.04
	Ca	1.70 ± 0.08	1.10 ± 0.05
Total		100.00	100.00

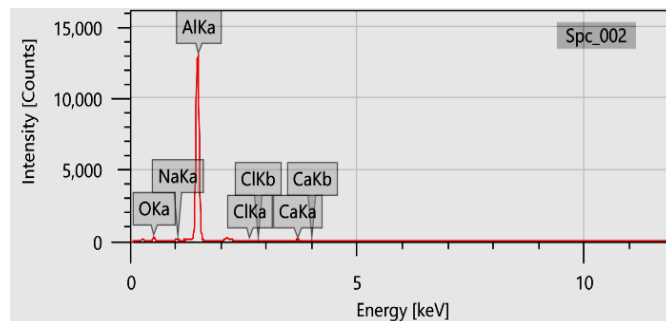


Fig. 3. EDX analysis for the commercial Al surface.

3.2. Electrochemical measurements

3.2.1. Tafel plot and the potentiodynamic polarization

The effect of sodium hydroxide and the addition of lithium hydroxide medium on the corrosion rate of the commercial aluminum sample was studied using Tafel polarization and the potentiodynamic techniques. Fig. 4 a and b represent the commercial aluminum's Tafel and potentiodynamic polarization curves in two percent (0 and 10) of 1M LiOH medium at 25 °C and in a sodium hydroxide solution of concentration 1M, respectively. Corrosion parameters such as corrosion potential (E_{corr}), and corrosion current density (i_{corr}) are obtained from the Tafel polarization curves. Results are tabulated in Table 3. The corrosion rate can be calculated using Eq. (1):

$$U_{Corr} = \frac{3270 \times M \times i_{Corr}}{\rho \times Z} \quad (1)$$

where 3270 is a constant that defines the unit of corrosion rate, i_{corr} is the corrosion current density in $A \text{ cm}^{-2}$, ρ is the density of the corroding material ($g \text{ cm}^{-3}$), M is the atomic mass of the metal, and Z is the number of electrons transferred per atom [16-18].

The negative shift in the corrosion potential (E_{corr}) with the increase in the presence of 10% LiOH indicates that the cathodic process is much more affected than the anodic process.

It should be noted that in the potentiodynamic

technique, the Al electrode is fully passivated in the case of 10% LiOH and not in the pure NaOH. This may be attributed to that the ionic mobility of Li is larger than that of Na.

It should be noted from calculating the value of the corrosion rate that the rate of corrosion decreases when using a solution of 10%LiOH compared with using pure NaOH, which is possible due to the Al electrode being fully passivated in the case of 10% LiOH and not in the pure NaOH. Furthermore, the effect of LiOH may be returned to the Li-ion activity and mobility compared to Na ions. This enables Li ions to be attracted to the polarized electrode more than Na.

3.2.2. EIS measurements

The corrosion behavior of the commercial aluminum electrode was also investigated by EIS techniques in various alkaline solutions of lithium hydroxide and sodium hydroxide mixture and pure sodium hydroxide medium. The impedance spectra were recorded and illustrated as Nyquist plots for the two cases. Nyquist plots for the commercial Al at the two different solutions at ambient temperature are shown in Fig. 5. The EIS results are tabulated in Table 3.

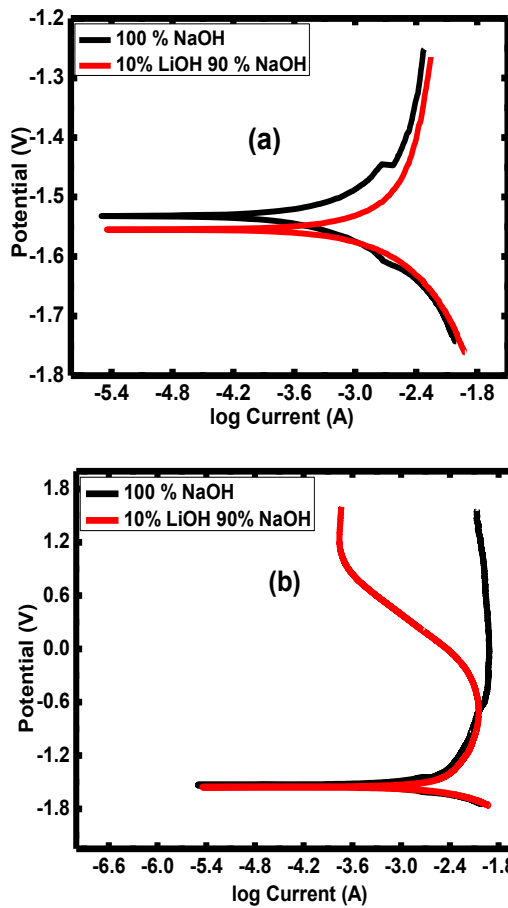


fig. 4. (a) Tafel polarization behavior of Al electrode in solutions of 1 M NaOH and 1M (90 percent NaOH+10 percent LiOH) at 25°C, (b) Potentiodynamic polarization behavior of Al electrode in solutions of 1 M NaOH and 1M (90 percent NaOH+10 percent LiOH) at 25°C.

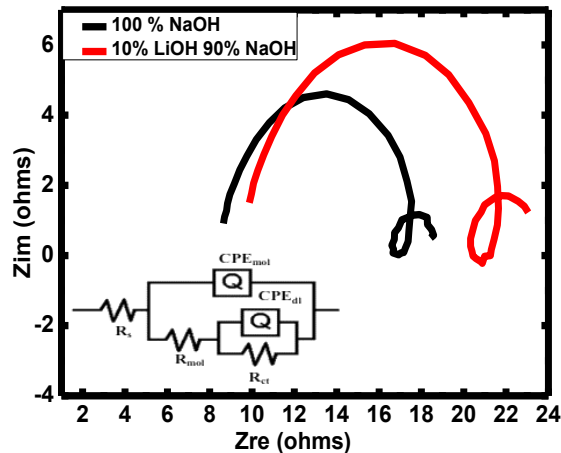


Fig. 5. The EIS measurements behavior of Al electrode in solutions of 1 M NaOH and 1M (90 percent NaOH+10 percent LiOH) at 25°C were accomplished by applying direct DC potentials of -100 and +100 mV, Ac potential amplitude of 10 mV, and frequencies ranging from 10000 Hz to 1 Hz, the equivalent electrical circuit used to emulate the impedance spectra are shown in the figure.

Table 3: Electrochemical corrosion parameters derived from Tafel polarization for the Al electrode in the presence of 1 M NaOH and 1M (90 percent NaOH+10 percent LiOH) at 25°C.

Aluminum	E_{corr} (V)	I_{corr} ($\mu A / cm^2$)	U_{Corr} (mm^2)
100% NaOH	-1.53	2730.7	29.76
90% NaOH + 10% LiOH	-1.55	2511.8	27.37

Table 4: EIS parameters for Al electrode in the solution of 1 M NaOH and 1M (90 percent NaOH+10 percent LiOH) at 25°C.

Aluminum	R_s	R_p	R_{ct}
100% NaOH	8.66	17.35	8.69
90% NaOH + 10% LiOH	9.88	21.32	11.44

As shown in Fig. 4, the impedance plot shows semicircles, indicating that the corrosion process is mainly charge transfer controlled. The depressed semicircles of the

Nyquist plots suggest the distribution of capacitance due to the inhomogeneous surface associated with the metal surface. The shapes of the curves are identical, and it contains a considerable capacitive loop at higher frequencies. The capacitive loop is attributed to the presence of a protective oxide film covering the surface of the aluminum metal. According to previous research, the capacitive loop corresponds to the interfacial reactions [19], particularly the reaction of aluminum oxidation at the interface of metal/oxide/electrolyte. The process includes the formation of Al ions at the metal/oxide interface and their transportation through the oxide/solution interface, where they are oxidized to Al^{3+} . At the oxide/solution interface, OH^- or O^{2-} ions are also formed.

On the other hand, the capacitive loop is attributed to the formation of the oxide film itself. Thereby, the origin of the inductive loop has often been attributed to the surface or bulk relaxation of species in the oxide layer. Also, the inductive loop may be attributed to the relaxation process obtained by adsorption and incorporation of hydroxide ions into the oxide film.

4 Conclusion

This work is devoted to studying the impact of adding a minor percentage of lithium-ion to sodium hydroxide solution on the electrochemical and corrosion behavior of aluminum electrodes to be applied for Al-air batteries. The study was accomplished using different techniques, such as EIS, Tafel, and Potentiodynamic polarization. The Potentiodynamic polarization manifested that the anodic line is shifted to a region for 10% LiOH than this of pure NaOH. At Tafel polarization E_{corr} was negatively shifted in the case of 10% LiOH, and accordingly, a decrease in the corrosion rate for 10% LiOH compared to the pure NaOH was observed. EIS data of both solutions show that the R_{ct} values decrease with pure NaOH. The SEM, EDX, and XRD analyses confirm the aluminum electrode's morphology, percentage, and phases.

References

[1] Yuxiang, Hu., Dan, Sun., Bin, Luo. & Lianzhou, Wang., Recent progress and future trends of aluminum batteries, *Energy Technol.*, **7(Jan)**, 86-106, 2019. <https://doi.org/10.1002/ente.201800550>.

[2] Ambroz, F., Macdonald, T.J., & Nann, T., Trends in aluminum-based intercalation batteries, *Advanced Energy Materials*, **7(Aug)**, 1602093, 2017. <https://doi.org/10.1002/aenm.201602093>.

[3] Liu, X., Zhang, P., & Xue, J., The role of micro-nanoscale AlSb precipitates in improving the discharge performance of Al-Sb alloy anodes for Al-air batteries, *J. Power Sources*, **425(June)**, 186-194, 2019. <https://doi.org/10.1016/j.jpowsour.2019.04.012>.

[4] Sovizi, M.R., Afshari, M., Jafarzadeh, K., & Neshati, J., Electrochemical and microstructural investigations on an as-cast and solution-annealed Al-Mg-Sn-Ga alloy as anode material in sodium chloride solution, *Ionics*, **23(Nov)**, 3073-3084, 2017. <https://doi.org/10.1007/s11581-017-2099-5>.

[5] Ren, J., Ma, J., Zhang, J., Fu, C., & Sun, B., Electrochemical performance of pure Al, Al-Sn, Al-Mg and Al-Mg-Sn anodes for Al-air batteries, *J. Alloys Compd.*, **808(Aug)**, 151708, 2019. <https://doi.org/10.1016/j.jallcom.2019.151708>.

[6] Liang, R., Su, Y., Sui, X.-L., Gu, D.-M., Huang, G.-S., & Wang, Z.-B., Effect of Mg content on discharge behavior of Al-0.05Ga-0.05Sn-0.05Pb-xMg alloy anode for aluminum-air battery, *J. Solid State Electrochem.*, **23(Jan)**, 53-62, 2019. <https://doi.org/10.1007/s10008-018-4093-x>.

[7] Gao, J., Li, Y., Yan, Z., Liu, Q., Gao, Y., Chen, C., Ma, B., Song, Y., & Wang, E., Effects of solid-solute magnesium and stannate ion on the electrochemical characteristics of a high-performance aluminum anode/electrolyte system, *J. Power Sources*, **412(Feb)**, 63-70, 2019. <https://doi.org/10.1016/j.jpowsour.2018.11.019>

[8] Du, X., Yan, Z., Wang, E., & Li, L., A high-performance air cathode with the hydrophobic pores distributed continuously and in gradient for zinc-air fuel cells, *Energy Technol.*, **6(May)**, 1860-1864, 2018. <https://doi.org/10.1016/j.apenergy.2019.03.004>.

[9] Tanski, T., Snopiński, P., Prusik, K., & Sroka, M., The effects of room temperature ECAP and subsequent aging on the structure and properties of the Al-3%Mg aluminium alloy, *Mater. Char.*, **133(Nov)**, 185-195, 2017. <https://doi.org/10.1016/j.matchar.2017.09.039>.

[10] Krol, M., Tanski, T., Snopiński, P., & Tomiczek, B., Structure and properties of aluminium-magnesium casting alloys after heat treatment, *J. Therm. Anal. Calorim.*, **127(Sep)**, 299-308, 2016. <https://doi.org/10.1007/s10973-016-5845-4>.

[11] Engler, O., Kuhnke, K., & Hasenclever, J., Development of intermetallic particles during solidification and homogenization of two AA 5xxx series Al-Mg alloys with different Mg contents, *J. Alloys Compd.*, **728(Dec)**, 669-681, 2017. <https://doi.org/10.1016/j.jallcom.2017.09.060>.

[12] Mokhtar, M., Zainal, M., Talib, M., Majlan, E. H., Tasirin, S. M., Ramli, W. M. F. W., Daud, & W. R. W., Sahari, J., Recent developments in materials for aluminum-air batteries: a review. *J Ind Eng Chem.*, **32(Dec)**, 1–20,

2015.

<https://doi.org/10.1016/j.jiec.2015.08.004>.

[13] Goel, P., Dobhal, D., & Sharma, R.C., Aluminum-air batteries: a viability review, *J. Energy Storage* **28(April)**, 10128, 2020.

<https://doi.org/10.1016/j.est.2020.101287>.

[14] Ilyukhina, A. V., Kleymenov B. V., Zhuk, & A. Z., Development and study of aluminum-air electrochemical generator and its main components [J]., *Journal of Power Sources*, **342(Feb)**, 741-749, 2017.

<https://doi.org/10.1016/j.jpowsour.2016.12.105>.

[15] Ren, J., Ma, J., Zhang, J., Fu, C., & Sun, B., Electrochemical performance of pure Al, Al-Sn, Al-Mg and Al-Mg-Sn anodes for Al-air batteries [J]., *Journal of Alloys and Compounds*, **808(Aug)**, 151708, 2019.

<https://doi.org/10.1016/j.jallcom.2019.151708>.

[16] Li, L., Liu, H., Yan, Y., Zhu, H., Fang, H., Luo, X., Dai, Y., & Yu, K., Effects of alloying elements on the electrochemical behaviors of Al-Mg-Ga-In based anode alloys [J]., *International Journal of Hydrogen Energy*, **44(May)**, 12073-12084, 2019.

<https://doi.org/10.1016/j.ijhydene.2019.03.081>.

[17] Afshari, M., Abbasi, R., Sovizi, & M. R., Evaluation of nanometer-sized zirconium oxide incorporated Al-Mg-Ga-Sn alloy as anode for alkaline aluminum batteries [J]., *Transactions of Nonferrous Metals Society of China*, **30(Jan)**, 90-98, 2020.

[https://doi.org/10.1016/s1003-6326\(19\)65182-4](https://doi.org/10.1016/s1003-6326(19)65182-4).

[18] Gao, J., Fan, H., Wang, E., Song, Y., & Sun, G., Exploring the effect of magnesium content on the electrochemical performance of aluminum anodes in alkaline batteries [J]., *Electrochimica Acta*, **353(Sep)**, 136497, 2020.

<https://doi.org/10.1016/j.electacta.2020.136497>.

[19] Ren, J., Ma, J., Zhang, J., Fu, C., & Sun, B., Electrochemical performance of pure Al, Al-Sn, Al-Mg and Al-Mg-Sn anodes for Al-air batteries, *J. Alloys Compd.*, **808(Nov)**, 151708, 2019.

<https://doi.org/10.1016/j.jallcom.2019.151708>.